JOURNAL OF MATERIALS SCIENCE 33 (1998) 2751–2762

Fatigue properties of jointed wood composites

Part I *Statistical analysis, fatigue master curves and constant life diagrams*

I. P. BOND
Department of Aerospace Engineering, University of Bristol, BS8 1TR, UK
M. P. ANSELL
School of Materials Science, University of Bath, BA2 7AY, UK
E-mail: I.P.Bond@bristol.ac.uk

The primary aim of this work was to assess the fatigue performance of scarf-jointed laminated wood composites used to manufacture wind turbine blades and establish simple fatigue design procedures. Laminates made from poplar (*Populus canadensis/serotina*), *Khaya* (*Khaya ivorensis*) and beech (*Fagus sylvatica*), incorporating typical scarf joints, were assessed under reversed loading ($R=-1$). Scarf joints were found to be great equalizers of fatigue performance for wood species with different static strengths. Poplar was investigated at several other R ratios ($+3$, -3, -0.84 and 0.33). The application of 95% survival probability limits derived from pooled data increases the statistical reliability of σ–N curves and gives an improved estimate of a material's minimum performance. The σ–N curves derived for all three wood species at $R=-1$ were normalized with respect to ultimate compressive strength values and found to be practically coincidental. This allowed the derivation of a master curve for a generic scarf-jointed wood laminate under reversed load conditions. This relationship was verified using data from the literature and found to be a good predictor of fatigue performance. The construction of simple triangulated constant life diagrams based on static tensile and compressive tests and fatigue testing at $R=-1$ brings about a rapid assessment of the overall fatigue performance of any wood composite. These can then be used in the fatigue design or life prediction of wood composites under cyclic loading.

1. Introduction

The commercial exploitation of wind energy initiated substantial research into optimizing and standardizing the criteria by which wind turbine blades (the most critical components of the machine) are designed and manufactured, with particular reference to fatigue performance.

Glass fibre-reinforced plastic (GFRP) is the most widely used material for rotor blades throughout the world. This is probably because it is relatively cheap, has good specific properties, is easy to fabricate and is well understood in terms of its behaviour under dynamic loading. However, laminated wood composite blades have been developed and used in the UK and the US since 1980, resulting in well-designed, low-cost wind turbine rotors. Wood used in this form has proved to be an excellent blade material and despite the continued development of GFRP and carbon fibre-reinforced plastic (CFRP) blades over the same period, this technology remains highly competitive, particularly for larger blades where its superior specific properties offer a distinct advantage [1, 2].

Wood is essentially a natural fibre-reinforced composite. It has a cellular, low-mass structure which gives it very good specific properties. It is cheap, readily available and performs well under fatigue loading. It is orthotropic in nature and its physical and mechanical properties are greatly dependent on moisture content. These limitations are overcome by a process of laminating thin veneers of wood with epoxy resin which reinforces and seals the wood in a way that is impossible with conventional paints. The veneers are end-jointed with glued scarf joints to minimize stress raisers. The scarf joints are staggered to avoid adjacent joints which would reduce strength. The addition of an encapsulating GFRP blade sheath helps resist splitting and shearing and provides a smooth aerodynamic surface. It also maintains a steady moisture content within the wood veneers. The anisotropy of wood means that shear and cross-grain stresses should be avoided, therefore the lay-up is such that the principal axis of loading is along the longitudinal or growth direction. Wood is weaker in compression than tension, thus compressive loading is

0022–2461

a dominant factor in blade design. Its low density and low strength mean that thick sections have to be used, providing excellent buckling resistance. The different species of wood show less variability in fatigue strength than different GFRP systems because fatigue strength depends mainly on the cellulose content reflected by the density of the wood [1, 3–5].

1.1. Wood fatigue

The world production of timber currently stands at around 10^9 tonnes per annum, making it a very important structural material [3]. Despite this high volume, information on the fatigue behaviour of wood is limited compared to metals or even advanced composite materials. This can probably be attributed to the major use of wood as a structural material in civil engineering where creep or duration of loading is the dominant design factor rather than fatigue. The occurrence of fatigue in wood was treated with scepticism until the advent of the Second World War [6]. This saw the increasing use of wood as an airframe material creating a sudden need for an understanding of its fatigue behaviour. The development of lightweight metals after the war meant a decline in the use of wood for this demanding application. The fatigue strength of wood is actually much higher than that of crystalline materials when compared to the static strength limit of the substance. This has led in the past to the rather widespread practice of ignoring fatigue properties.

Much of the literature regarding the fatigue of wood has concerned testing in flexure [7]. This is a legacy of wood being used as beams, flooring, etc., in the construction industries. In addition, the lack of sophisticated testing equipment available to early workers resulted in most testing being carried out under deflection control, load control being difficult to achieve. Wood being a viscoelastic material is susceptible to creep and reduction in modulus with time, therefore, under deflection control, peak loads gradually decline over the test period allowing indefinite continuation with no visible sign of failure [6]. Much of the work performed in this way must be treated with suspicion, particularly at long lifetimes.

An extensive review of wood fatigue literature has been carried out by Tsai and Ansell [8] and supplemented by Bonfield and Ansell [9]. Readers are referred to these two papers for detailed study of wood fatigue. Both solid and laminated wood have been tested in flexure and rotating bending by numerous workers [8, 10–19]. Although there is a large degree of uncertainty regarding the actual fatigue strengths of various wood species, the consensus seems to be that solid and laminated wood do not greatly differ in fatigue behaviour. In complete contrast, Sterr [20] concluded that laminated wood had a higher fatigue strength than solid wood and Ota and Tsubota [21] concluded that the resin type used for laminating also affected fatigue strength.

A further area of debate is the form of the σ–N curve for wood fatigue. Kommers [13] suggests an asymptotic value is approached at low stress levels, although his data were obtained using constant deflection testing and a test frequency of 30 Hz which introduces the problem of adiabatic heating, giving rise to a change in wood properties. Lewis [22] also assumes from his work on tensile axial fatigue that extrapolation of data lines show an asymptotic trend. Most of the published data is for less than 5×10^6 cycles so the case for extrapolation to 10^7 cycles and beyond is, at best, questionable.

The same factors that affect static mechanical properties also affect fatigue life. For example, moisture content, temperature, density, grain angle and defects will all have an effect and have been investigated by several workers [11, 17, 19, 23–25].

Bonfield *et al.* [26–29] and Johnson [24] carried out a great deal of axial fatigue testing at various R ratios. Bonfield and Ansell [26] went on to derive a constant life diagram for *Khaya ivorensis* after testing at R ratios of -1, -2, -10 and 0.1. In a later paper [27], the same authors looked at the effects of specimen size and block loading. They concluded that size had negligible effect on fatigue life at $R = -1$ although size is probably an important variable in bending. Block loading was used to try and verify Miner's Rule [30] ; the result, however, was critically dependent on σ–N data interpretation.

1.2. Jointed wood

The effect of joints, whether glued, bolted or nailed, on mechanical performance, is of great interest to designers and users of wooden structures. Most wooden structures will require the use of several members necessitating the use of joints.

Maku and Sasaki [19] examined, in rotating bending fatigue, various configurations of scarf- and butt-jointed wood laminates. Scarfed specimens performed similarly to unjointed specimens in both static and fatigue, whilst butt-jointed specimens performed much more poorly. Bonfield *et al.* [29] carried out a similar study comparing various joint configurations incorporating butt, scarf, overscarf and underscarf joints in *Khaya ivorensis*, Black Italian poplar and European beech. Little difference was found in the performance of Khaya, all joint configurations, except overscarf, having similar failure modes. In the case of beech and poplar, all scarf-jointed specimens outperformed those containing butt joints. Lewis [22] compared solid and scarf-jointed Douglas Fir and found no decrease in fatigue life with the presence of joints, provided the lower static strength was accounted for.

Bohannan and Kanvik [31] studied two types of finger-jointed Douglas fir. They found that after 30×10^6 cycles at $R = 0.1$, the specimens possessed approximately 40% of their static strength and approximately 80% of the strength of 1:8 slope scarf-jointed specimens that had undergone similar testing.

1.3. Fatigue design

Critical to the success of a dynamically loaded structure is its fatigue design which relies on the understanding of fatigue behaviour at all R ratios

($\sigma_{min}/\sigma_{max}$). This can be determined from a constant life or a Goodman diagram where mean stress versus alternating stress is plotted for numerous different R ratios and bell-shaped curves representing constant lives can be constructed. The generation of such diagrams normally requires a large number of tests of representative material to provide σ–N curves from which constant life data can be derived. Previous work at the University of Bath [32] generated a comprehensive fatigue database which led to the derivation of a constant life diagram for unjointed *Khaya* laminate. However, joints in a large wood structure are a practical requirement. Scarf joints are easy to fabricate and provide good load transfer with little stress concentration. An assessment of their performance in fatigue is necessary for reliable and safe fatigue design of wood composite wind turbine blades. A method of easily assessing the global fatigue performance of jointed wood composite systems is a principal aim of this paper.

Principal changes to a wood composite, such as use of an alternative wood species or resin type, require a sensible number of tests to give a clear indication of structural fatigue performance. The effect on fatigue life of smaller changes to the manufacturing method, such as joint type, joint configuration, components of the GRP skin, etc., could be assessed by minimal testing. If the general bell shape of the constant life diagram in Fig. 1 is assumed to be typical for all structural wood species, then imposing a triangle with corners at ultimate tensile strength (*UTS*), $R = 1$ and ultimate compressive strength (*UCS*) values creates a conservative constant life diagram that fits within the original comprehensive curve.

Measurement of the *UTS* and *UCS* and generation of a σ–N curve at $R = -1$ and statistical treatment of the data to improve its reliability allows the rapid generation of simplified constant life diagrams which offer a safe estimate of fatigue life. These diagrams can subsequently be used for the fatigue design and prediction of lifetime to failure of blade materials. A method of statistically treating fatigue data is discussed below.

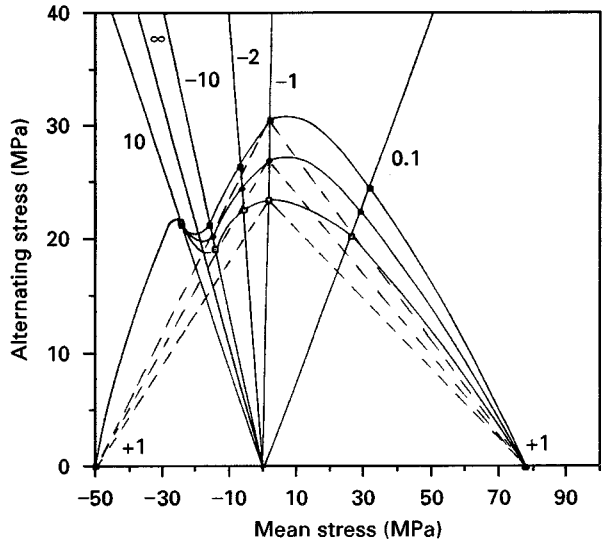

Figure 1 Comprehensive constant life diagram for *Khaya ivorensis* overlaid with simplified triangulated constant lifelines. (□) 10^7 cycles, (●) 10^6 cycles, (■) 10^5 cycles.

2. Data analysis and statistical treatment

2.1. Regression of σ–N data

The calculation of regression curves is invaluable in determining the relationships between stress and cycles to failure at a particular R ratio. It must be noted that in the case of σ–N data, the applied stress, σ, is the independent variable and the number of cycles to failure, N, is the dependent variable. This must be taken into account when performing any statistical analysis on the data.

In the cases of log–log σ–N plots, several log N values were obtained for each σ level tested and thus median value of $\log N$ have been used in the regression analysis according to the recommendation in *ASTM E*206 [33].

2.2. Statistical intervals

Any measurement of a material property is liable to show scatter. In the case of fatigue testing, this scatter is generally large, often spanning three orders of magnitude. This problem of scatter has made it common practice to estimate and construct an interval around the data which, with a high degree of probability, contains a specific value of interest.

Three different types of statistical intervals are commonly used.

(i) A *confidence interval* is an estimate of an interval which will contain the population mean, μ. The sample mean, $\bar{x}$, is an estimate of the unknown population mean, μ, but differs because of sampling fluctuations. The confidence interval contains μ with a specific degree of probability, known as the confidence level. The confidence limits are calculated from $\bar{x} \pm C_m(n)s$, where $c_m(n)$ is a tabulated value depending on the degree of probability required, m, and the number of observations in the sample, n. s is the standard deviation (S.D.) of the sample.

(ii) A *prediction interval* is an interval calculated to contain all of a number of future observations with a certain degree of probability. Prediction limits are calculated using the formula $\bar{x} \pm c_{P,k,\gamma}(n)s$, where $c_{P,k,\gamma}(n)$ is a tabulated prediction constant, c_p, for γ, the percentage probability to include k future observations and is dependent on n, the number of observations in the sample.

(iii) A *tolerance interval* is an interval calculated to include at least a stated proportion, P, of the population with a stated probability, γ. For a normal distribution, if μ, the mean, and σ, the standard deviation, of the population are known, it can be stated that a certain percentage of the population will lie within the interval $\mu \pm A\sigma$, where A is a tabulated value dependent upon the proportion of the population that is to be included in the interval. However, if only $\bar{x}$, the sample mean, and s, the sample S.D., are known, then it can only be stated that an interval will contain a certain proportion of a population with a specified probability. For example, we can say with 95% confidence

that 95% of the population will lie within this interval. Tolerance limits are calculated using the formula $\bar{x} \pm c_{T,P,\gamma}(n)s$, where $c_{T,P,\gamma}(n)$ is a tabulated tolerance constant, which depends on the proportion of the population to be included, P, the percentage confidence that this interval includes this proportion, γ, and the number of observations in the sample, n. These probability constraints can be chosen to reflect the degree of certainty that is required to be enforced upon the data. The constants necessary for the derivation of these limits are available in the literature, for example, Natrella [34].

Sometimes it is only of interest to estimate a value above or below which a certain proportion of a population will lie. In this case it is only necessary to use one-sided upper or lower tolerance limits which are calculated in the same way as above; however, the $c_{T,P,\gamma}(n)$ values must be different to accommodate the change in statistical requirements.

2.3. One sided 95% tolerance limits applied to pooled data

A one-sided 95% tolerance limit can describe a lower limit to data, above which one can say with 95% confidence that there is a 95% survival probability for any future sample. In the case of σ–N data for any R ratio, there is a need for a statistical limit that defines a minimum boundary below which the majority of experimental data will not be expected to lie. This boundary can subsequently be used in the fatigue design of components subjected to dynamic loading. A 95% survival probability was chosen because it provides a precise statistical lower boundary which is not too stringent when applied to widely scattered fatigue data.

Pooling data creates a larger sample and thus improves statistical accuracy. It can be done by plotting cycles to failure, N, and applied peak stress, σ_{pk}, data on log–log axes and then subjecting the data to a 50% median linear regression analysis to generate Equation 1

$$\log N = c - m \log \sigma_{pk} \quad (1)$$

The experimental values of σ_{pk} are then transformed using Equation 2 to form data set σ^*. The standard deviation, S, can then be calculated for this data set of $\log \sigma^*$

$$\log \sigma^* = \log \sigma_{pk} + \log N/m \quad (2)$$

The lower limit value is calculated by

$$\text{low lim} = C_{T,P,\gamma}(n)\, Sm \quad (3)$$

where $C_{T,P,\gamma}(n)$ is a tabulated value for a one-sided lower tolerance limit as described above.

Finally, the 95% survival probability boundary curve is expressed by

$$\log N = c' - m \log \sigma \quad (4)$$

where $c' = c - \text{low lim}$.

3. Experimental procedure

3.1. Sample lay-up and geometry

The laminated wood composites used in this investigation were made from African mahogany (*Khaya ivorensis*), black poplar (*Populus canadensis/serotina*) and European beech (*Fagus sylvatica*). Test panels were fabricated from rotary cut veneers. The laminating procedure used a gap-filling epoxy resin ("SP Ampreg 20") with filler additions to avoid excessive absorption of the resin into the porous wood. Laminates of four 5 mm and five 4 mm veneers thick were produced with a single scarf joint in each layer with a spacing of 30 mm. After lay-up the panels were vacuum consolidated at room temperature for several hours. Finally, an outer skin of 1600 g $m^{-2} \pm 45°$ non-woven glass/epoxy overlaid with a layer of 290 g m^{-2} woven 0°/90° glass/epoxy was applied to each panel face. Dogbone specimens with a gauge length of 150 mm and a gauge width of 18 mm (Fig. 2) were produced using a profiled jig and router. Prior to testing, the samples were stored in a controlled environment to maintain a moisture content of 12% in the wood.

To study the effect joints have no mechanical performance, laminates were made incorporating two different joint types. The first was 1:7 slope scarf joint bonded with epoxy resin ("SP125") and the second was a micro-finger joint (length = 9 mm, pitch = 3 mm) using a water-based, room-temperature cure phenol–resorcinol–formaldehyde resin.

3.2. Mechanical testing

3.2.1. Static testing

Tensile testing of all samples was carried out using a 200 kN servohydraulic test machine. Aluminium end-tabs were bonded to the sample ends using epoxy resin to prevent samples from being crushed and pulling out of the grips. Tensile testing was carried out by applying a ramp load and setting a trip to trigger as the movement of the hydraulic ram exceeded a certain pre-set limit, i.e. as the sample failed. The maximum tensile load the sample sustained was recorded using a hold function on the load-cell display.

The long, thin specimen geometry of the jointed samples (Fig. 2) meant that for compressive testing an anti-buckling guide was necessary. This was constructed from thick aluminium plate lined with polytetra fluoroethylene (PTFE) tape to reduce friction and small pieces of wood veneer were used as packing to hold the guide in position over the sample gauge

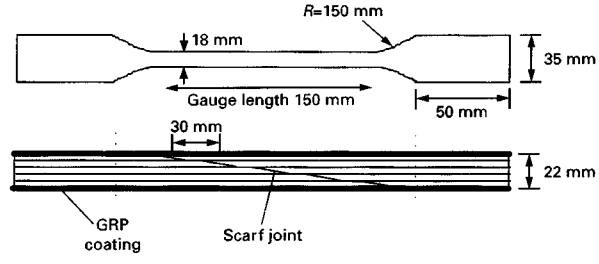

Figure 2 Test specimen profile and joint geometry.

length and protect the sample edges. This device allowed free longitudinal movement of the specimen but restricted any lateral movement. Testing was carried out in exactly the same way as described above, except the loading was in compression and the hold function was set to record the minimum compressive load sustained before failure.

3.2.2. Fatigue testing

Fatigue data at stress ratios of $R = -1$, -0.84, -3, $+3$ and 0.33 were obtained by axially testing samples in load control using a 200 kN Mayes servohydraulic test machine. The long, thin specimen geometry of the dogbone samples required the use of an anti-buckling guide at $R = -3$ and $+3$. A plastic sheet was used to form an enclosed chamber around the sample during testing in which the relative humidity was maintained at 65%. A constant rate of stress application (RSA) of 400 MPa s^{-1} was selected for all the fatigue testing. This was because a change in peak stress level for a test at the same frequency will result in a change in RSA (Fig. 3a). The RSA has a considerable effect on the fatigue life of wood due to its viscoelastic behaviour and so a fixed RSA/variable frequency condition was adopted (Fig. 3b). Adiabatic heating of the samples is a concern during fatigue testing because cyclic loading of wood results in hysteresis leading to heat generation. Frictional heating will also occur in locations such as joint surfaces. These two heating effects, coupled with the insulating property of wood, lead to considerable heat build-up in the samples, particularly as the frequency of stress application increases. Thus 8Hz was deemed to be the maximum frequency for testing because at this level adiabatic heat generation causes a change in wood properties.

This use of a fixed RSA is in agreement with the literature [35] which suggests that due to frequency effects encountered in many composite materials, all static and fatigue testing for a particular material should be carried out at the same rate and at a level which avoids any hysteretic effects. An RSA of 400 MPa s^{-1} was chosen because it was sufficiently high to provide a practical testing timescale without leading to adiabatic heating of samples under test.

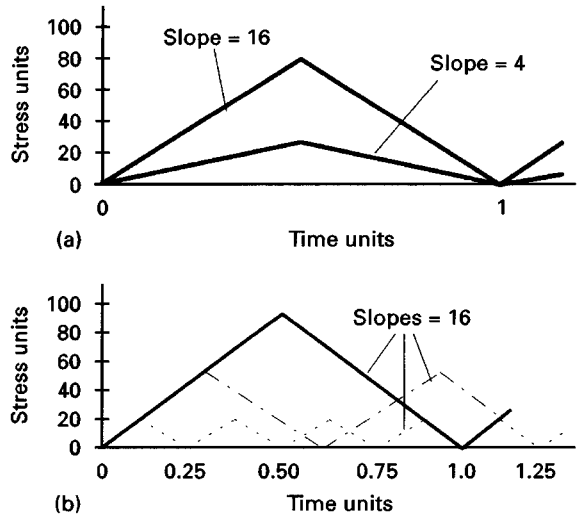

Figure 3 The effect on stress rate and frequency of cyclically testing at (a) a fixed frequency and (b) a constant rate of stress application.

4. Results

4.1. Axial testing in monotonic tension and compression

The strength of wood is mainly a function of its density, which reflects the cellulose content in the material. The results of testing in tension and compression gives rise to strengths which strongly correlate with the wood densities. Poplar is the lightest wood (380–530 kg m^{-3}), *Khaya* the intermediate (450–580 kg m^{-3}) and beech the heaviest (670–710 kg m^{-3}). This order is mirrored in both the compressive and tensile test results.

Table I compares the UTS and UCS values of scarf-joined poplar. The presence of good-quality joints was found to have a lesser effect on the ultimate compressive strength than on the ultimate tensile strength as expressed by the degree of scatter in the data. This results in the 95% survival probabilities for tensile and compressive strength being of similar magnitude.

Table II compares the UTS and UCS values of scarf-jointed and unjointed *Khaya*. When compared to unjointed material, scarf joints appear to cause a

TABLE I Strength data for scarf-jointed poplar laminate

	UCS	UTS
Mean (MPa)	− 52.51	62.58
S.D. (MPa)	− 4.94	9.31
95% Surv. prob. (MPa)	− 38.76	37.38
Coeff. of variation (%)	11.04	14.88
No. of samples	11	12
Specific strength (MPa $kg^{-1} m^{-3}$)	0.115	0.138

TABLE II Strength data for scarf and unjointed *Khaya* laminate

	UCS		UTS	
	Unjointed	Scarf	Unjointed	Scarf
Mean (MPa)	− 49.47	− 54.16	81.80	76.16
S.D. (MPa)	− 2.77	− 5.98	9.3	5.59
95% Surv. prob. (MPa)	− 43.41	− 37.52	58.88	59.41
Coeff. of var. (%)	5.60	11.04	11.37	7.35
No. of samples	32	11	17	9
Specific strength (MPa $kg^{-1} m^{-3}$)	0.096	0.105	0.159	0.148

reduction in the scatter of the UTS data due to their action as stress concentrators which dominates the inherent variability in the wood. Conversely, for the compressive strength, the presence of joints increases the scatter in the data. This can be attributed to the different numbers of samples tested and also the fact that different sample geometries were investigated. Table III compares UTS and UCS data for scarf-jointed beech. The tensile performance shows a high degree of scatter which is reflected in the low value for the 95% survival probability.

The results suggest that in monotonic tension, joints in wood laminates have a detrimental effect, acting as initiation sites for tensile failure. However, this loss in performance can be minimized by stringent quality control during manufacture. Under compressive load, joints seem to have little effect on the failure mode of the wood and thus are less detrimental to the wood strength. Compressive failure occurs in a localized damage region which appears in a plane perpendicular to the loading direction with no obvious interaction with joints. Generally, joints are a great leveller of a wood's strength and the stronger the wood, the more difficult it is to maintain that strength once joints are present.

TABLE III Strength data for scarf-jointed beech laminate

	UTS	UCS
Mean (MPa)	84.66	− 69.29
S.D. (MPa)	14.18	− 4.98
95% tol. limit (MPa)	49.19	− 56.39
Coeff. of var. (%)	16.75	7.19
No. of samples	16	14
Specific strength (MPa $kg^{-1}m^{-3}$)	0.123	0.100

4.2. Axial constant amplitude fatigue testing at various *R*-ratios

An important force behind this work was the economic and environmental need to change the design of wood composite wind turbine blades from using *Khaya ivorensis* (a tropical hardwood) to a more benign wood source. Several candidate woods are studied [29] with poplar and, to a lesser extent, beech being chosen for further investigation. The comprehensive fatigue database produced for *Khaya* in a previous research effort [32] meant that comparable data would be needed for poplar if it were ever to be implemented in blade manufacture. Thus, six σ–N curves were produced, five for poplar, one for beech and the $R = -1$ curve for *Khaya* [32] was further supplemented.

4.2.1. Results for scarf-jointed poplar

Fig. 4 is a log–log σ–N plot for scarf jointed poplar which has been subjected to fatigue loading at $R = -1$, -0.84, -3, $+3$ and 0.33. All the curves except that for $R = 0.33$ have fatigue data co-plotted with UCS data, because in each of these conditions the compression component of the cyclic loading is a higher proportion of the UCS than the tensile component is of the UTS. It is, therefore, presumed the compressive component is the predominant factor in the damage-accumulation process. For the $R = 0.33$ data, the loading is all tensile and thus UTS data are

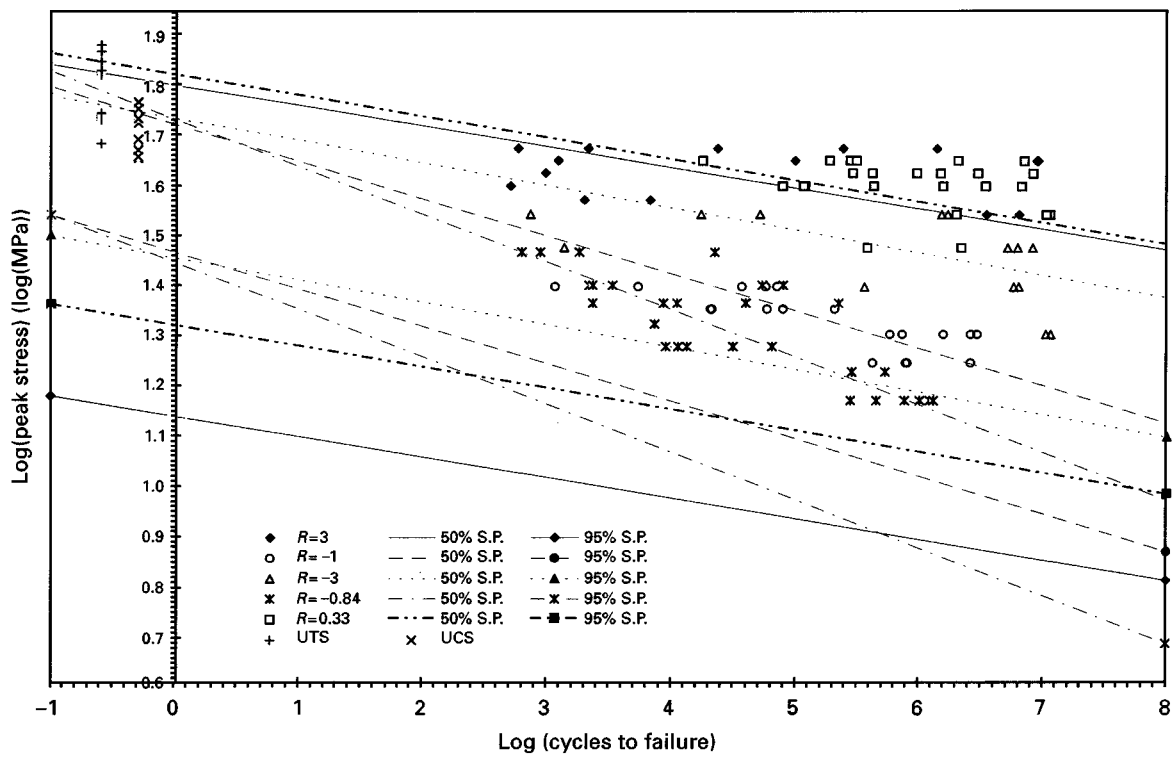

Figure 4 Log–log σ–N curves for scarf-jointed poplar fatigue tested at $R = -1$, -0.84, -3, $+3$, $+0.33$. The diagram shows 50% probability of failure median regression curves.

included. Each curve shows a 50% probability of failure regression curve for median values of the data at each stress level tested and a 95% survival probability curve obtained using the method described in Section 2.

For the data obtained at $R = -1$ (reversed loading), scatter of up to two orders of magnitude is observed. The R ratio of -0.84 (tension–compression) corresponds to the ratio of UCS/UTS for poplar. As Fig. 4 shows, the regression curve has the steepest gradient of all the R ratios investigated indicating the highest rate of damage accumulation occurs at the highest rate and thus compressive and tensile damage are possibly taking place simultaneously. Relatively few data points were obtained at $R = -3$ (compression–tension). However, they do include two runout points of 10^7 cycles at a $\sigma_{min} = 20$ MPa implying a possible fatigue limit at this stress level. Fatigue testing at $R = +3$ (compression–compression) gave a very shallow gradient regression curve which suggests that compressive stresses up to 35 MPa can be applied and still result in $> 10^6$ cycles to failure. It could also be inferred that a fatigue limit is approached at a minimum stress value of 30 MPa where lifetimes approach or exceed 10^7 cycles. The scatter in the data is extremely large for some stress levels, for example at 47.5 MPa over three orders of magnitude. Generally, the data lie within a narrow stress region with widely varying lives to failure for the same applied stress. Again the regression curve has a shallow gradient for results at $R = 0.33$ (tension–tension). A fatigue limit is implied below 35 MPa where three runouts of 10^7 cycles were observed. There is a large degree of scatter in the data.

Fig. 5 shows a normalized σ–N plot for poplar comparing all the R ratios tested, $R = -1$, -0.84, -3, $+3$ and 0.33. The positional order of the σ–N curves is, from the top, $R = +3$, $R = 0.33$, $R = -3$, $R = -1$ and $R = -0.84$. This clearly shows the detrimental effect of having a mixed-mode load regime which passes through zero stress because the shallowest gradients are found near single-mode compressive ($R = +3$) or tensile ($R = 0.33$) loading. The R ratio -0.84 (tensile–compressive) denotes a condition where both tensile and compressive damage mechanisms are equally active. Correspondingly, this R ratio shows the steepest gradient for its σ–N curve as damage is accumulating in both modes.

4.2.2. Results for scarf-jointed Khaya

The fatigue performance of unjointed *Khaya* has been extensively characterized at numerous R ratios in previous work [9, 32] so it was not deemed necessary to test *Khaya* extensively at these same R ratios. However, some testing was essential to allow comparison with the alternative wood species under the same test conditions and to provide some indication of the changes in behaviour due to the presence of the joints.

Fig. 6 is a log–log σ–N plot for scarf-jointed *Khaya* which has been subjected to $R = -1$ fatigue loading. Again, the fatigue data are co-plotted with the UCS data as explained in Section 4.2.1. and have a 50% probability of failure regression curve and a 95% survival probability curve fitted to the data, derived according to the method described in Section 2. The data exhibit a degree of scatter up to two orders of magnitude of life. A fatigue limit may be present below a minimum stress level of ≈ 20 MPa where data points were clustering around 3–4 million cycles and a runout of 10^7 cycles were measured.

4.2.3. Results for scarf-jointed beech

Fig. 7 is a log–log σ–N plot for scarf-jointed beech which has been subjected to $R = -1$ fatigue loading. The fatigue data are co-plotted with the UCS data as explained in Section 4.2.1 and have a 50% probability of failure regression curve and a 95% survival probability curve fitted to the data, derived according to the method described in Section 2. The scatter in the

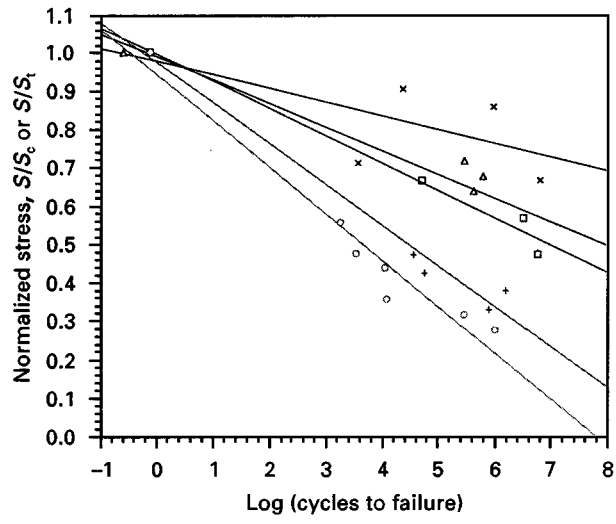

Figure 5 Normalized σ–N plot for scarf-jointed poplar at all R ratios based on median fatigue lives. R: (×) + 3, (△) + 0.33, (□) − 3, (+) − 1, (○) − 0.84.

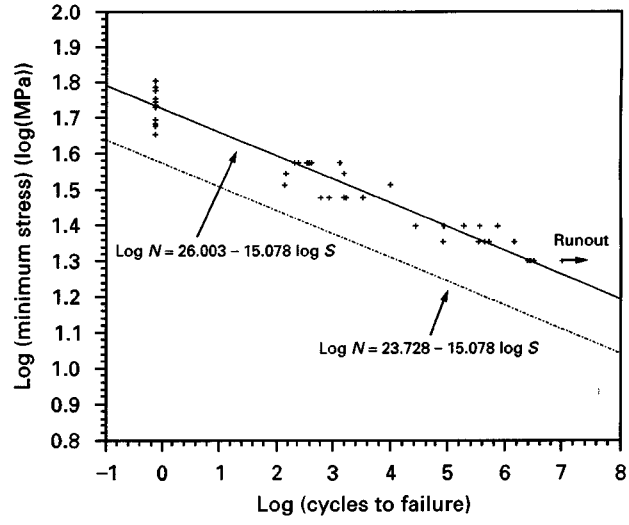

Figure 6 Log–log σ–N curves for scarf-jointed *Khaya* fatigue tested at $R = -1$. (—) 50% probability of failure median regression curves, (–·–) 95% survival probability (+) experimental data.

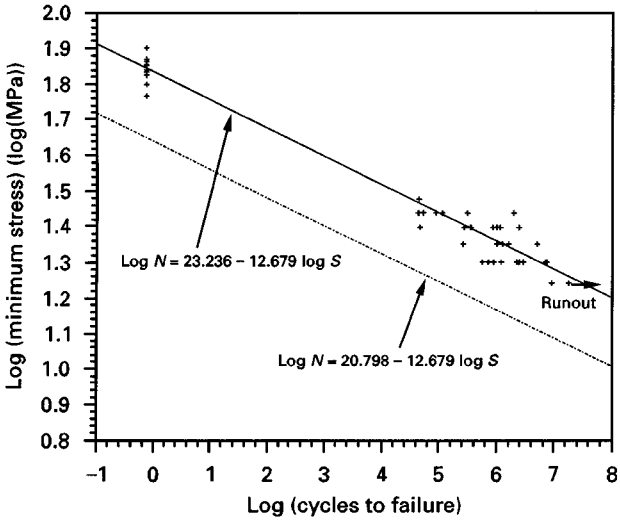

Figure 7 Log–log σ–*N* curves for scarf-jointed beech fatigue tested at $R = -1$. (—) 50% probability of failure median regression curves, (–·–) 95% survival probability (+) experimental data.

data is up to two orders of magnitude of life with a fatigue limit suggested below 17.5 MPa by the recording of a failure at 9×10^6 cycles and a runout of greater than 10^7 cycles.

4.3. Discussion of fatigue performance and failure

Comparison of all three scarf-jointed species, poplar, *Khaya* and beech, tested under $R = -1$ fatigue loading suggests that wood composite performance is remarkably similar. Interpolation of allowable minimum stresses from regression curve fits to the data reveals that poplar and *Khaya* behave very similarly throughout the whole fatigue range. Beech, although a stronger wood, shows a more rapid decline in fatigue strength with increasing cycles and thus at high lifetimes its stress allowables are close to the other two species. Once again it would appear that the presence of joints is a great equalizer of fatigue performance for wood species of different static strength.

Poplar, being the preferred choice of blade material for economic reasons, was characterized under fatigue loading to a greater extent. The ratio $R = -0.84$ was found to be the most demanding on the poplar laminate. This R ratio corresponds to the ratio of UCS/UTS for poplar, therefore, the compressive and tensile components of each cycle are proportionally the same when compared to their respective static strengths. The resulting steep σ–*N* curve suggests that both damage mechanisms are occurring simultaneously, producing the poorest fatigue performance. Similar R ratios for other materials would be useful in establishing an understanding of "worst case" cyclic loading and Ansell *et al.* [36] studied this interesting load condition when applied to several forms of fibre-reinforced composite material.

In general, fatigue failure under mixed-mode loading is observed at stress levels well below the scatter band of the respective static strengths suggesting that this is more detrimental to wood laminates than all tensile or all compressive loading. This behaviour is in agreement with studies on fibre-reinforced plastics by Curtis [35] and Poppen and Bach [37]. The critical factor in determining the onset of failure is the stress range, Δσ, of the cycle. For a given applied stress, mixed-mode loading will always have a larger Δσ than single-mode loading. These larger Δσ values lead to the dissipation of more hysteresis energy per stress–strain cycle in the viscoelastic wood and thus must lead to a higher rate of damage accumulation.

From the single-mode fatigue loading results for poplar at $R = +3$ and 0.33 (Fig. 4) and beech at $R = 0.33$ (Fig. 7), fatigue failure is observed at stress levels near to or coincident with the scatter of UCS or UTS values. This results in a large spread of lifetimes to failure as "weak samples" show poor fatigue performance at the same stress levels where "strong samples" are more impressive. This interdependence of static and fatigue strength is exhibited in many fibre-reinforced polymer composites [38, 39] and has been labelled the Strength–Life Equal Rank Assumption or SLERA, and appears equally applicable to laminated wood composites. The theory states that for a given specimen its rank in static strength is equal to its rank in fatigue life under single-mode loading.

A large amount of static and fatigue data for scarf-jointed Douglas fir/epoxy wood composites has been generated in the USA under the administration of NASA and funded by the US Department of Energy [40]. They found that all tensile ($R = 0.1$) and all compressive ($R = 10$) fatigue loading resulted in markedly different σ–*N* curve gradients, the lines converging at approximately 10^8 cycles. This contrasts with Fig. 4 where the results from testing scarf-jointed poplar indicate that for single-mode loading ($R = 0.33$ and 3) the σ–*N* curves are almost coincidental. These differences are probably attributable to the larger joint area (higher stress transfer capability) and thinner 2.5 mm veneer (larger volume fraction of resin) in the Douglas fir material tested in the USA.

5. Derivation of σ–*N* master curve at $R = -1$

Fig. 8 is a direct comparison of three species, *Khaya* poplar and beech, after fatigue testing at $R = -1$ [2].The data have been normalized with respect to the respective UCS values. The regression curves are almost coincidental which implies that once the respective compressive strength is taken into account, all three scarf-jointed species give a remarkably similar performance under reversed axial fatigue loading. There is, therefore, some justification for deriving a general σ–*N* master curve for scarf-jointed wood laminate behaviour under reversed loading conditions, as a function of the compressive strength, σ_c

$$\sigma = \sigma_c[0.97 - 0.103 \log N] \quad (5)$$

where N is the cycles to failure, σ_c the *UCS*, and σ the allowable minimum stress.

Bonfield [32] has provided static and fatigue data for several wood species, including Douglas fir, Baltic pine and birch. Regression curves have been applied

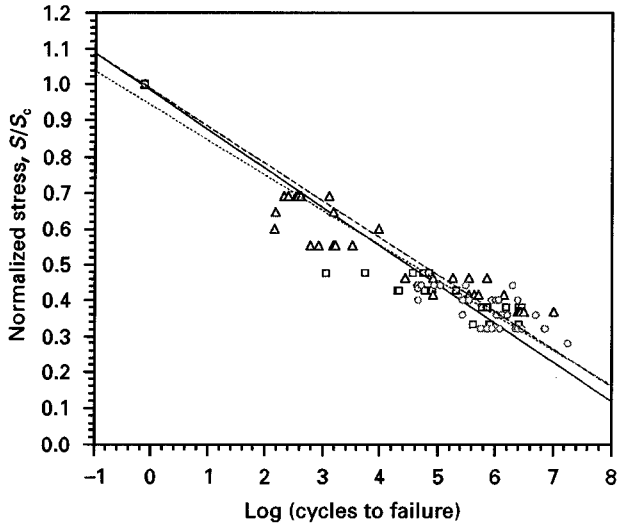

Figure 8 Normalized σ–*N* curves for (△, - - -) *Khaya*, (□, - -) poplar and (○, - - -) beech at $R = -1$. 50% survival probability regression curves. (—) $y = 0.982 - 0.108x$, (- - -) $y = 0.941 - 0.097x$, (— — —) $y = 0.985 - 0.103x$.

TABLE IV σ–*N* relationships

	Master curve derived σ–*N* relationships	Experimentally derived σ–*N* relationships
Douglas fir	$\sigma = 59.17 - 6.283 \log N$	$\sigma = 60.29 - 5.678 \log N$
Baltic pine	$\sigma = 38.80 - 4.120 \log N$	$\sigma = 43.00 - 3.831 \log N$
Birch	$\sigma = 53.35 - 5.665 \log N$	$\sigma = 55.56 - 5.618 \log N$

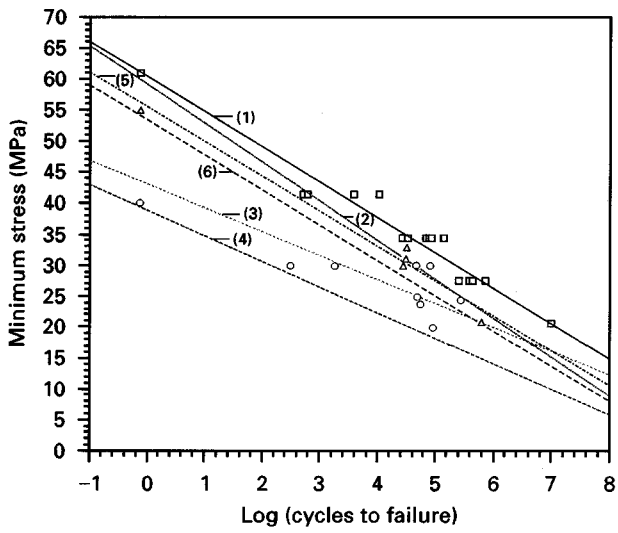

Figure 9 Comparison of empirical and master curve derived relationships for (1,2) (□) Douglas fir, (3,4) (○) Baltic pine and (5,6) (△) birch: (1,3,5) 50% regression, (2,4,6) master curves.

to the data based on 50% probability of failure and the resulting relationships are shown below. If the UCS values for these wood species (Douglas fir = 61 MPa, Baltic pine = 40 MPa and birch = 55 MPa) are used with the master curve equation above, the σ–*N* relationships shown in Table IV result.

In Fig. 9, the master curve derived relationships are seen to correlate reasonably well with the regression curves through the data. The Douglas fir and Baltic

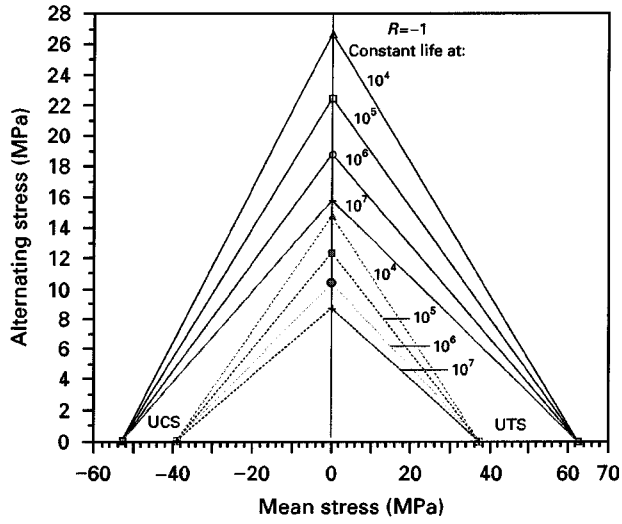

Figure 10 Simplified constant life diagram for scarf-jointed poplar derived from (△, □, ○, +) 50% probability median regression and (▲, ■, ●, *) 95% survival probability curves.

pine relationships show a divergence with increasing numbers of cycles. The Baltic pine shows the worst correlation of the three data groups, probably due to the large scatter within the data set. The birch data (although only five data points) correlate most closely with the master curve derived relation. The discrepancy between the two relationships is to be expected, as the experimental data were obtained using unjointed material, whereas the master curve relationships predict the behaviour of scarf-jointed material. Comparison of the pairs of relationships shown in Table IV displays a good correlation, implying that the master curve relationship could be applied to wood laminate systems in general.

6. Constant life diagrams

A simplified, triangulated constant life diagram based on fatigue data at $R = -1$, UTS data and UCS data for scarf-jointed poplar (Fig. 4) is shown in Fig. 10. The lines define combinations of mean and alternating stress, σ_a and σ_m, respectively, for lifetimes to failure of 10^4, 10^5, 10^6 or 10^7 cycles. The full lines represent a 50% survival probability and the broken lines represent a 95% survival probability. The decrease in allowable combinations of σ_a and σ_m when statistical limits are applied is quite marked and this is a result of the original σ–*N* data containing large scatter and relatively few data points.

A constant life diagram for poplar incorporating *R* ratios of 0.33, −0.84, −1, −3, +3, and UCS and UTS data is shown in Fig. 11. The approximately parabolic form of the diagram becomes distorted at the ratio $R = -0.84$. The allowable σ_a and σ_m values at this ratio seem inconsistent with the general form of the diagram, particularly at lifetimes above 10^4 cycles. This is a result of the steep gradient regression curve applied to the σ–*N* data (Fig. 4). As discussed in Section 4.3, this *R* ratio coincides with a condition where both compressive and tensile damage modes occur with equal likelihood. Another feature of the

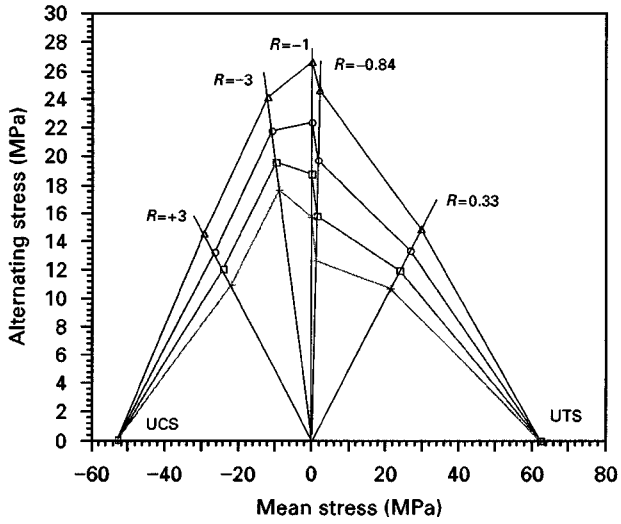

Figure 11 Comprehensive constant life diagram for scarf-jointed poplar derived from 50% probability median regression curves: (△) 10^4, (○) 10^5, (□) 10^6, (+) 10^7.

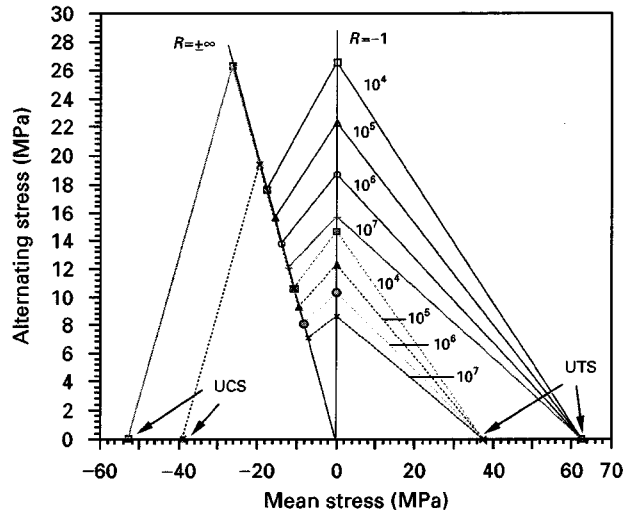

Figure 13 Simplified constant life diagram for scarf-jointed poplar with a compression loading of $(\sigma_m + \sigma_a) = UCS$. (□, △, ○, +) 50% probability median regression, (■, ▲) 95% survival probability, (●, ×) 50% survival probability.

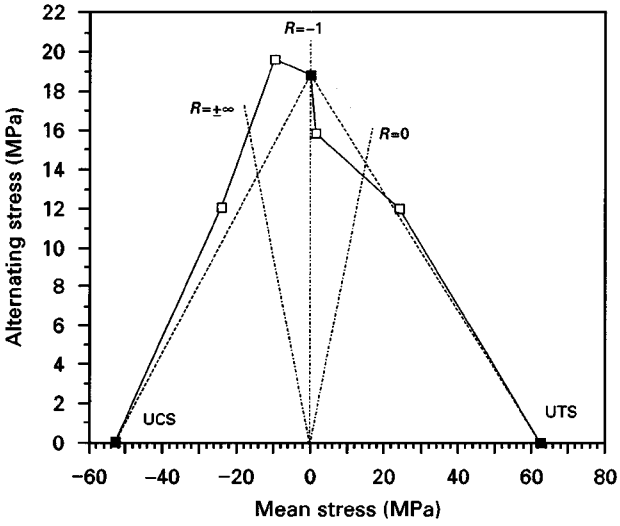

Figure 12 Comparison of (□) comprehensive and (■) simplified constant life lines for scarf-jointed poplar at 10^6 cycles.

diagram is that as the lifetime to failure increases, the apex in the family of iso-cycle curves moves from the reversed load condition ($R = -1$) towards an increasingly compressive cyclic loading. This reflects the superior fatigue performance of wood laminates under compressive load, e.g. $R = +3$, where the lowest rate of damage accumulation is observed (Fig. 5).

A comparison of a simple triangulated constant life line taken from Fig. 10, and a comprehensive lifeline from Fig. 11, both at lifetime of 10^6 cycles, is made in Fig. 12. As can be seen there is a marginal difference in geometry. The triangulated iso-cycle curve is slightly optimistic in tension–compression loading ($-1 < R < 0$), and is slightly conservative in compression–tension ($-\infty < R < -1$) and compression–compression ($+1 < R < +\infty$) loading. It is clear that the use of simplified, triangulated constant lifelines as a method of characterizing a laminated wood composite in fatigue does not lead to an excessively optimistic or conservative understanding of its fatigue behaviour.

From the results of fatigue testing poplar at $R = +3$, Figs 4 and 5, it can be argued that compression–compression fatigue of wood laminates does not occur outside the scatter of UCS values. This is supported by results from fatigue testing of full-scale wood composite wind turbine blades [41] where failure under cyclic loading was only achieved after the application of stresses within the scatter range of the compressive strength of the wood.

If this argument is carried forward and considered applicable to constant life data, the result is a markedly different diagram, Fig. 13. The compression–compression iso-cycle lines of the Fig. 10 have been replaced by values which are derived from the equations below.

$$(\sigma_m + \sigma_a) = UCS_{mean} \quad (6a)$$

$$(\sigma_m + \sigma_a) = UCS_{95\%S.P.} \quad (6b)$$

where σ_m is the mean stress, σ_a the alternating stress, UCS_{mean} the mean compressive strength and $UCS_{95\%S.P.}$ the 95% survival probability compressive strength.

The iso-cycle lines for 10^4, 10^5, 10^6 and 10^7 cycles are coincident. This creates an irregular constant life diagram but considerably increases the allowable stresses under all compressive loading and increases the overall area of the fatigue performance envelope. The assumption that fatigue does not occur under a compressive load regime is justified, but further study of the behaviour of wood under this load regime is required to provide a degree of certainty.

In theory, the master curve for fatigue performance of a wood composite at $R = -1$ (Section 5) could be used, with appropriate UTS and UCS data, to generate simple triangulated constant life diagrams for any wood species. This would allow generation of a safe basic fatigue performance envelope derived with only minimal static testing.

7. Conclusion

Under constant amplitude cyclic loading at $R = -1$, laminated wood composites made from poplar, *Khaya* and beech gave fatigue performances which were very similar when normalized with respect to UCS. Scarf-jointed poplar was investigated over a range of other R ratios ($+3$, -3, -0.84 and 0.33). Single-mode loading, $R = +3$ (compression–compression) and $R = 0.33$ (tension–tension), resulted in very similar behaviour with large scatter in the data and almost coincident regression curves. In both cases it was found that stress levels which caused fatigue were very near or overlapped the scatter band of the respective static strengths. The R ratio of -0.84, equal to the UCS/UTS ratio was investigated as it is a condition at which the likelihood of tensile and compressive damage occurring is equal. The σ–N relationship at $R = -0.84$ has the greatest slope, suggesting that both modes of damage (tensile and compressive) were occurring simultaneously.

The application of 95% survival probability lower limits to σ–N curves using pooled data increases their statistical reliability and reduces the number of data points necessary for deriving a characteristic σ–N curve. Their subsequent use in simplified constant life diagrams increases safety margins over and above the simple triangulated procedure and gives a reliable estimate of a material's minimum performance level.

The σ–N data at $R = -1$ for three different wood composites were normalized with respect to their UCS values and found to be practically coincidental. This allowed the derivation of a master curve for scarf-jointed wood laminate fatigue performance at $R = -1$. The master curve was also verified using fatigue data from the literature. The large degree of scatter throughout all the fatigue data would suggest that the Strength–Life Equal Rank Assumption, where a sample occupies the same rank in terms of its static strength and its lifetime to failure, is very applicable to laminated wood composites.

A test and analysis methodology has been demonstrated that allows a rapid assessment of the fatigue performance of new or modified blade materials. By performing only static tensile and compressive tests and fatigue testing at an R ratio of -1 (reversed loading), a simplified, triangulated constant life diagram can be constructed and used in the fatigue design or life prediction of blades where scarf joints are routinely used to join the ends of wood veneer sheets. This provides benefits in that many samples can be static and fatigue tested at one R ratio in a short period of time and at a lower cost than a comprehensive test programme.

Acknowledgements

The authors are very grateful to the UK Department of Trade and Industry for funding this work via the Energy Technology Support Unit under Contract W/44/00287 and the CEC DG-XVII for funding as a partner in the JOULE-II programme under Contract JOU2-CT92-0085.

References

1. M. P. ANSELL, M. HANCOCK and P. W. BONFIELD in "Proceedings of the International Timber Engineering Conference, edited by J. Marcroft Vol. 4 (TRADA, Buckingham, 1991) pp. 194–202.
2. M. HANCOCK, Wind Energy Group, Report for DTI no. WEG/R038/6201, March 1994.
3. J. M. DINWOODIE, "Timber – Its Nature and Behaviour" (Van Nostrand Reinhold, London, 1981).
4. H. E. DESCH, "Timber – Its Structure, Properties and Utilisation", 6th Edn (Macmillan, London, 1981).
5. J. BODIG and B. A. JAYNE, "Mechanics of Wood and Wood Composites" (Van Nostrand Reinhold, New York, 1982).
6. W. C. LEWIS, in "Proceedings of ASTM 46" (American Society for Testing and Materials, Philadelphia, 1946) pp. 814–835.
7. G.H. KYANKA, *Int. J. Frac.* **16** (1980) 609.
8. K. T. TSAI and M. P. ANSELL, *J. Mater. Sci.* **25** (1990) 865.
9. P. W. BONFIELD and M. P. ANSELL, *ibid.* **26** (1991) 4765.
10. K. T. TSAI and M. P. ANSELL, in "Proceedings of the 6th BWEA Wind Energy Conference – Wind Energy Conversion-1984", edited by P. Musgrove (Cambridge University Press, Cambridge, 1984) pp. 239–255.
11. K. T. TSAI and M. P. ANSELL, in "Proceedings of the 7th BWEA Wind Energy Conference – Wind Energy Conversion-1985", edited by A. Garrad (Mechanical Engineering Publications, London, 1985) pp. 285–292.
12. K. T. TSAI, PhD thesis, University of Bath (1987).
13. W. J. KOMMERS, US Forest Products Research Laboratory, Report no. 1327 (U.S. Department of Agriculture, Madison, Wisconsin, 1943).
14. A. G. H. DIETZ and H. GRINSFELDER, *Trans ASME* (1943) pp. 187–191.
15. G. JENKINS, Bristol Aircraft Ltd, Structures and Materials Laboratory Report No. 171–76B-3040 (1962).
16. N. IMAYAMA and T. MATSUMOTO, *J. Jpn Wood Res. Soc.* **16** (1970) 319.
17. Y. IBUKI, H. SASAKI, M. KAWAMOTO and T. MAKU, *J. Jpn Soc. Test. Mater.* **11**(101) (1962) 103.
18. F. B. FULLER and T. T. OBERG, *J. Aeronaut. Sci.* March (1943) 81.
19. T. MAKU and H. SASAKI, *Mokuzai Kenkyu* **31** (1963) 23.
20. R. STERR, *Holz. als Roh Werkstoff* **21**(2) (1963) 47 (Trans. no. 171. Canada Department of Forest Products Research Branch).
21. M. OTA and Y. TSUBOTA, *J. Jpn Wood Res. Soc.* **12** (1966) 26.
22. W. C. LEWIS, *Proc. US Forest Prod. Res. Soc.* **5** (1951) 221.
23. A. C. SEKHAR, N. K. SUKLA and V. K. GUPTA, *J. Nat. Bldg. Org.* **8**(4) (1963) 36.
24. P. E. JOHNSON, "Design of test specimens and procedures for generating material properties of Douglas Fir/Epoxy laminated wood composite material" Final Report NASA-CR-174910; DOE/NASA-0286-1; UDR-TR85-45 DEN3-286; DE-AI01-79ET-20320 850700, March 1982-March 1985 (1985).
25. W. C. LEWIS, US Forest Products Laboratory Report no. 2236 (U.S. Department of Agriculture, Madison, Wisconsin, 1962).
26. P. W. BONFIELD and M. P. ANSELL, in "Proceedings of the 10th BWEA Wind Energy Conference – Wind Energy Conversion-1988", edited by D.J. Milborrow (Mechanical Engineering Publications, London, 1988) pp. 377–383.
27. *Idem.*, in "Proceedings of the European Wind Energy Conference – EWEC'89" (Peter Peregrinus, Amsterdam, 1989) pp. 406–410.
28. *Idem.*, in "Proceedings of the 13th BWEA Wind Energy Conference – Wind Energy Conversion-1991", edited by A. Garrad, D. Quarton, V. Fenton (Mechanical Engineering Publications, London, 1991) p. 311–316.
29. P. W. BONFIELD, I. P. BOND, C. L. HACKER and M. P. ANSELL, in "Proceedings of the 14th BWEA Wind Energy Conference – Wind Energy Conversion-1992", edited by B. Clayton (Mechanical Engineering Publications, London, 1992) p. 243–250.
30. M. A. MINER, *Trans. ASME* **67** (1945) A159.

31. W. BOHANNAN and K. KANVIK, US Forest Products Research Laboratory Research Paper FPL114 (U.S. Department of Agriculture, Madison, Wisconsin, 1969).
32. P. W. BONFIELD, PhD thesis, University of Bath (1991).
33. ASTM E206 (1972) "Fatigue testing and the statistical analysis of fatigue data", (American Society for Testing and Materials, Philadelphia, PA, 1972).
34. M. G. NATRELLA, "Experimental Statistics. Handbook 91", US Department of Commerce, (National Bureau of Standards, US Government Printing Office, Washington, DC, 1963).
35. P. T. CURTIS, *J. Strain Anal.* **24**(4) (1989) 235.
36. M. P. ANSELL, I. P. BOND and P. W. BONFIELD, in "Proceedings of the 9th International Conference on Composite Materials", Vol. V (Edited by A. Miravete, Woodhead Publishing, University of Zaragoza, 1993) pp. 692–99.
37. M. POPPEN and P. W. BACH, "Fatigue testing using the Wisper sequence", ECN Report, ECN-RX-91-077 (The Netherlands Energy Research Foundation, Petten, Holland, 1991).
38. P. C. CHOU and R. CROMAN, *J. Compos. Mater.* **12** (1978) 177.
39. P. M. BARNARD, R. J. BUTLER and P. T. CURTIS, *Int. J. Fatigue* **10**(3) (1988) 171.
40. D. A. SPERA, J. B. ESGAR, M. GOUGEON and M. D. ZUTECK, "Structural properties of laminated Douglas Fir/Epoxy composite material" DOE/NASA 20320-76, NASA Reference Publication 1236, US Department of Commerce, National Technical Information Service, N91-10127 (Washington, D.C. 1991).
41. M. HANCOCK and M. BOND in "Proceedings of the 17th BWEA Wind Energy Conference - Wind Energy Conversion-1995", edited by B. Clayton (Mechanical Engineering Publications, London, 1995) pp. 275–81.

Received 24 September 1997
and accepted 13 February 1998